Influence of Gd on structural and impedance properties of multiferroic composites: $BiFeO_3$-$PbTiO_3$

Nilaya K. Mohanty, Ajay K. Behera, Santosh K. Satpathy, Banarji Behera[*], Pratibindhya Nayak

Materials Research Laboratory, School of Physics, Sambalpur University, Jyoti Vihar, Burla 768019, Odisha, India

[*]Corresponding author. Tel: (+91) 66-3243-1719; E-mail: banarjibehera@gmail.com

ABSTRACT

The Gd-modified $BiFeO_3$-$PbTiO_3$ composites i.e. $0.5BiGd_xFe_{1-x}O_3$-$0.5PbTiO_3$ (BG_xF_{1-x}-PT) with x=0.00, 0.05, 0.10, 0.15, 0.20, were prepared by mixed oxide method at high temperature. The structural study reveals that the composites showed tetragonal crystal structure at room temperature and tetragonality (c/a ratio) of composites decrease with increase in Gd concentration. The average crystallite size of the composites was found to be in the range of 30-89 nm. Surface morphology of the composites was studied by scanning electron microscopy (SEM). The Goldschmidt tolerance factors of the composites were found to be in the range of 0.989-0.976. The nature of Nyquist plot confirmed the presence of both bulk and grain boundary effects, and non-Debye type of relaxation process occur in the composites. The activation energy of the composites was found to be in the range 0.13-1.38eV. The analyses of ac conductivity data obey the universal agreement with Jonscher's power law. Further, the explanation of conduction mechanism through correlated barrier hopping (CBH) model was discussed. Copyright © 2015 VBRI Press.

Keywords: Ceramics; X-ray diffraction; complex impedance; electrical properties.

Introduction

In recent years, the development of multiferroic materials have been great interest for potential applications such as spintronics, electromagnetic interference filter, data storage media, multiple state memories transducers, actuators etc. This is due to the coexistence of both ferroelectric and ferromagnetic order in the same phase [1-3]. The $BiFeO_3$ (BFO) is one such multiferroic material which has ferroelectric phase at Curie temperature (T_C~850 ^oC) and antiferromagnet phase at Neel temperature (T_N~310 ^oC) [4, 5]. However, its low remanent magnetization, low electrical resistivity, high dielectric loss and relatively high leakage current are the main limitations for possible device application. The existence of relatively high conductivity of BFO is believed to have due to the reduction from trivalent Fe^{3+} ions towards more divalent Fe^{2+} ions, which creates oxygen vacancies for charge compensation. Hence, special attention has been laid on synthesis of BFO with some other perovskite such as $PbTiO_3$, $BaTiO_3$, $SrTiO_3$ and $Pb(Fe, Nb)O_3$, $Pb(Ti,Zr)O_3$ etc, [6-10] in order to improve the multiferroic properties. The achievement of this above perovskite structure triggered the research interest on bismuth ferrite-lead titanate $(1-x)BiFeO_3$-$xPbTiO_3$ during early 1960s [11, 12], which ultimately realized a stable perovskite phase with low coercive field E_c [8]. The search finally yields the system $(1-x)$ $BiFeO_3$-$xPbTiO_3$ with the

desired structural stabilization and enhanced electrical properties due to the morphotropic phase boundary (MPB). The MPB of the system separates the tetragonal and rhombohedral phases at x=0.3 [12]. The existence of weak ferromagnetism in this system has also reported [12, 13]. Moreover, the substitution of rare earth (RE^{3+}) ion on Bi-site in BFO found to exhibit the improve multiferroics properties as well as ceases the oxygen ion vacancy, and evaporation of Bi_2O_3 [14-16]. It is also reported that most of the transition metal (TM) group element with aliovalent ions substituted on Fe-site of BFO yields the enhanced electrical resistivity and magnetic properties with reduction in the valence fluctuation in Fe [17]. The doping of TM group element at Fe-site shows a change in Fe-O-Fe super exchange interaction which affects the magnetic properties [18]. The improvement seen in the introduction of TM group element at Fe-site, we have tried to substitute the RE ion Gd^{+3} at Fe sites of the composite $0.5BiFeO_3$-$0.5PbTiO_3$ to expect the change in impedance properties as well as the electrical and magnetic properties through RE^{3+}-Fe^{3+} coupling.

Experimental

Gd doped solid solutions of $BiFeO_3$-$PbTiO_3$ (BFO-PT) $(0.5BiGd_xFe_{1-x}O_3$-$0.5PbTiO_3)$ (BGF-PT) with x = 0.00, 0.05, 0.10, 0.15, 0.20) were prepared by the mixed oxide

method. The high purity precursors: Bi_2O_3 and Gd_2O_3 (99.99 %, M/s Spectrochem Pvt. Ltd., India), Fe_2O_3 ($\geq$ 99%, M/s Loba Chemicals, Pvt. Ltd., India), PbO ($\geq$95%, M/s Spectrochem Pvt. Ltd., India) and TiO_2 ($\geq$ 99% Merck Specialties Pvt. Ltd., India) were carefully weighed in a suitable stoichiometric proportion. The materials were mixed thoroughly in air for 2 h and in methanol for another 2 h. The mixed powders were calcined in a high purity alumina crucible at an optimized temperature of 800 °C for 6 h in an air atmosphere. The formation of composites were studied by an X-ray diffraction technique at room temperature with a powder diffractometer (D8 Advanced, Bruker, Karlsruhe, Germany) using CuK$_\alpha$ radiation (λ = 1.5405 Å) in a wide range of Bragg's angles 2θ ($20^0 \leq \theta \leq 80^0$) with a scanning rate of 3°/min. Then the calcined powder was mixed with polyvinyl alcohol (PVA) to make the pellet. The PVA acts as a binder to reduce the brittleness of the pellet and burnt out during sintering. The cylindrical pellets were formed with dimension of 10 mm diameter and 1-2 mm of thickness at pressure of 3.5×10^6 N/m^2 using a hydraulic press. These pellets were sintered at 800 °C for 6 h in an air atmosphere. The sintered pellets were polished by fine emery paper to make both the surfaces flat and parallel. To study the electrical properties of the composites, both flat surfaces of the pellets were electroded with air-drying conducting silver paste. After electroding, the pellets were dried at 150 °C for 4 h to remove moisture, if any, and then cooled to room temperature before taking any electrical measurement. The surface morphology of the sintered pellet was studied at room temperature by a scanning electron microscopy (SEM) technique using a scanning electron microscope (JSM-6480, JEOL). The electrical parameters (impedance and capacitance) of the composites were measured using an LCR meter (HIOKI, Model-3532) in the frequency range of 10^2-10^6 Hz from 25 to 450 °C.

Results and discussion

Structural study

Fig. 1(**a-b**) shows the room temperature XRD pattern of the system $0.5BG_xF_{1-x}$-0.5PT with x = 0.00, 0.05, 0.10, 0.15, 0.20. All of the diffraction peaks were indexed in different crystal system and unit cell configurations.
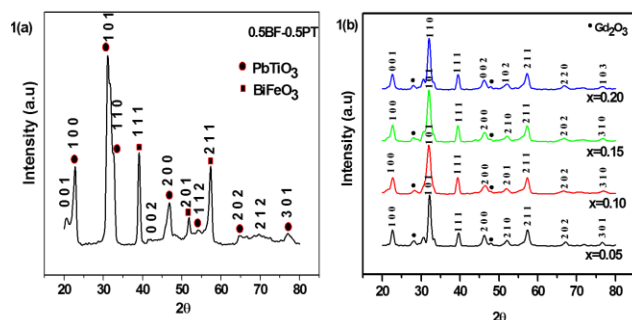
**Fig. 1** (a-b). XRD patterns of $BiGd_xFe_{1-x}O_3$-PbTiO$_3$ (x=0.00, 0.05, 0.10, 0.15, 0.20).

The tetragonal crystal system was confirmed on the basis of good agreement between observed (obs) and

calculated (cal) inter planar spacing d ($\sum \Delta d = d_{obs} - d_{cal}$ = minimum). As shown in **Fig 1** (**a**), the peak positions for undoped 0.5BF-0.5PT (x=0.00) sample was in good agreement with reported one [**19-21**]. The peaks of $BiFeO_3$ and $PbTiO_3$ phase have been shown in the figure and the peak positions were well matched with JCPDS no 72-2112, 74-1947. The extra peaks were observed at 2θ~28.15 and 48.0 as shown in **Fig 1**(**b**) may be due to the doping of rare earth Gd and well matched with the individual Gd_2O_3 [**22**]. The lattice parameters of the selected systems were refined using the least-squares sub-routine of a standard computer program package "POWD" [**23**], and given in the **Table 1**.

Table 1. Values of lattice parameter of $BiGd_xFe_{1-x}O_3$-PbTiO$_3$ (x=0.00, 0.05, 0.10, 0.15, 0.20).

Parameters (A^0)	x=0.00	x=0.05	x=0.10	x=0.15	x=0.20
a	3.8748	3.9141	3.9145	3.9212	3.9251
c	4.2989	4.0157	4.0150	3.9925	3.9812
c/a	1.1095	1.0260	1.0257	1.0182	1.0143

It is observed that the c/a ratio decreases from 1.10 to 1.01 with increase in Gd concentration similar to the results for La substituted on Bi site of (1-y)BF-yPT [**24**].
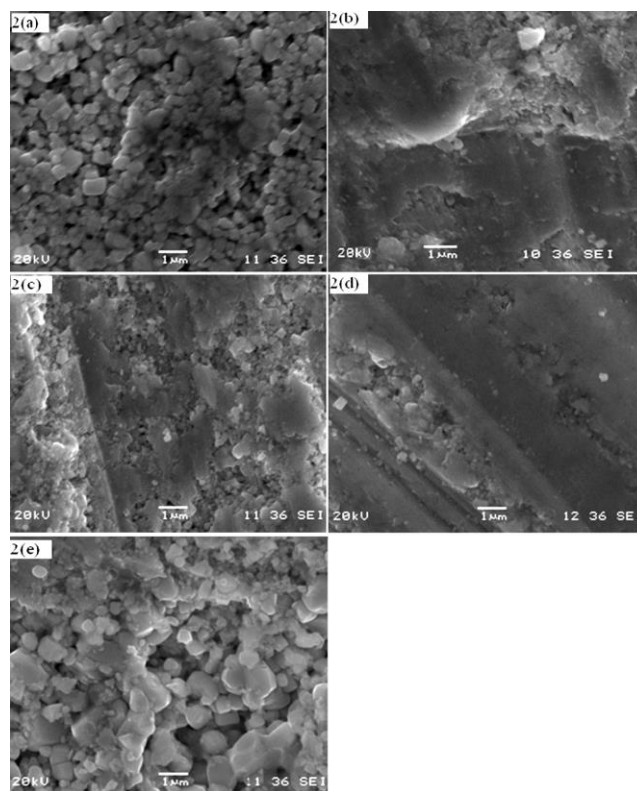
Fig. 2. (a-e). SEM micrographs of $BiGd_xFe_{1-x}O_3$-PbTiO$_3$ (x=0.00, 0.05, 0.10, 0.15, 0.20).

This decreasing trend of c/a may suggest the tetragonal distortion in the composites. Further, the lattice constant 'a' slowly increases with increase in Gd concentration. This may be due to the fact that the ionic radius of Gd^{3+} is larger than Fe^{3+} which induces more distortion on Fe site to accommodate larger ions. The crystallite size (P) of the composites were roughly estimated from the broadening of the XRD peaks (in a wide 2θ range) using the Scherrer's

equation [25] $P = K\lambda / \left(\beta_{1/2} \cos\theta_{hkl} \right)$, where the constant K = 0.89, λ = 1.5405 Å, and $\beta_{1/2}$ is the peak width of the reflection at half intensity. The average value of P were found to be 54, 89, 30, 41 and 44 nm for x = 0.00, 0.05, 0.10, 0.15 and 0.20 respectively. **Fig 2** (**a-e**) shows the SEM micrograph of the sintered pellets of the studied composites for x=0.00, 0.05, 0.10, 0.15, 0.20. The grains are homogeneously distributed throughout the surface of the samples for x=0.00 and 0.20 with less voids and the corresponding grain size found to be in the range of 0.3-0.7 µm. However, it is not possible to evaluate the average grain size for the concentration 0.05-0.15 as the grain looks hazy.

The tolerance factor (*t*) concept for single perovskite (ABO$_3$) system given by Goldschmidt [26] is also adopted to our studied composites with the doping of rare earth ions on Fe site as,

$$t = \frac{\frac{r_{Bi} + r_{Pb}}{2} + r_0}{\sqrt{2}\left[\left(\frac{(1-x)r_{Fe} + x\,r_{Gd}}{2}\right) + \frac{r_{Ti}}{2} + r_0\right]}$$

where, r_{Bi}, r_{Pb}, r_{Fe}, r_{Gd}, r_{Ti} and r_0 are the ionic radii of the respective ions. The proposed t values for ideal ABO$_3$ with undistorted structure is 1 whereas the value of t<1 or t>1 refers for distorted ABO$_3$ structure with tilt or rotation of BO$_6$ octahedron [27, 28]. Further, based on the extensive structural data, it has been shown that for t values lying between 0.985<t< 1.06 and 0.964<t<0.985 are expected to have untilted and antiphase tilt structure respectively. However, for t<0.964 are expected to show both in phase and anti-phase tilting [29, 30]. The tolerance factor for our studied perovskite composites are evaluated by considering Shannon ionic radii [31] and found to be 0.989, 0.986, 0.983, 0.979, and 0.976 for x=0.00, 0.05, 0.10, 0.15, and 0.20 respectively. The range of tolerance factor of the studied composites for different concentration of Gd may be considered to exist in both untilted and tilted perovskite structure. Further, the substitution of Gd ion with higher ionic radius (0.938 Å) in place of Fe with lower ionic radius (0.645 Å), we expect the consequence of stretching on Bi/Pb-O bond due to the compression of bond along Gd/Fe-O.

Complex impedance study

The complex impedance spectroscopy (CIS) [32] is a unique, powerful and well known tool to characterize the transport properties. Generally, the contribution of bulk, grain boundary and electrode effect in the materials can be evaluated by separating the real and imaginary components of the complex impedance parameters. This may be calculated from the basic formalism as: $Z^*(\omega) = Z' - jZ''$ where $Z' = |Z|\cos\theta$ and $Z'' = |Z|\sin\theta$ and complex electric modulus as: $M^*(\omega) = M' + jM''$, $M' = \omega C_0 Z''$, $M'' = \omega C_0 Z'$, where ω is the angular frequency (2πf),

$C_0 = \varepsilon_0 S / d$ is the geometric capacitance, ε_0 is the permittivity of the free space, S is the area and, d is the thickness of the sample.
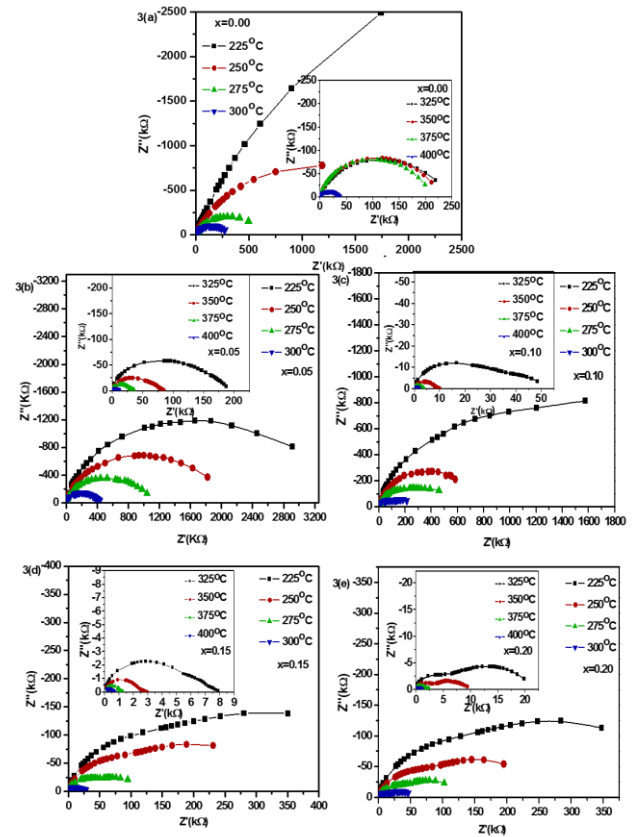

Fig. 3. (a-e). Nyquist plot of BiGd$_X$Fe$_{1-X}$O$_3$-PbTiO$_3$ (x=0.00, 0.05, 0.10, 0.15, 0.20).

Fig. 3 (a-e) shows the Nyquist plot (Z' vs. Z") at different temperatures (225 – 400 °C) in the wide frequency range for all the composites with concentration x=0.00-0.20. A single semicircular arc is observed (for x=0.00 and 0.05) which confirms the presence of bulk effect only. But for x=0.10 and 0.15, a semicircular arc along with the tendency of second semicircular is observed. For x=0.20 (at 325-400 ^{0}C), there is a clear evidence of two semicircles, which indicates the presence of both grain and grain boundary effect in the composites. This nature of plot suggests that the electrical response contains at least two relaxation phenomenon for x=0.10-0.20 at different frequencies. The grain boundary effect is observed on increasing the Gd concentration. The Nyquist plots also show the depressed semicircles whose centre lies below the real axis and exhibit non-Debye type of relaxation phenomenon in the composites [33]. Further, it is observed that the bulk resistance decreases with increase in temperature as well as Gd concentration. This clearly shows the negative temperature coefficient of resistance (NTCR) behavior. Similar behavior has also been observed for other Gd doped double perovskite structure [34]. The impedance data for all the composites with composition x=0.00-0.20 was fitted with equivalent circuit and well matched with the model R$_1$(C$_1$(R$_2$(Q(R$_3$W))))(C$_2$R$_4$) (for

x=0.00) and $R_1(C_1(R_2(Q(R_3(C_2R_4)))))$ (for x=0.05-0.20) at 400 °C as shown in **Fig. 1** (**a-e**) [**ESI**], where R, C, Q and W are resistance, capacitance, constant phase element and Warburg element respectively. The fitting parameters are summarized and shown in **Table 1** [**ESI**] with χ^2 value.

Fig. 2 (**a-e**) [**ESI**] shows the variation of Z' and M' with frequency at different temperatures for all the composites. It is clearly seen that the values of Z' decreases with increase in temperature and confirms the NTCR behavior as observed in **Fig. 3** (**a-e**).
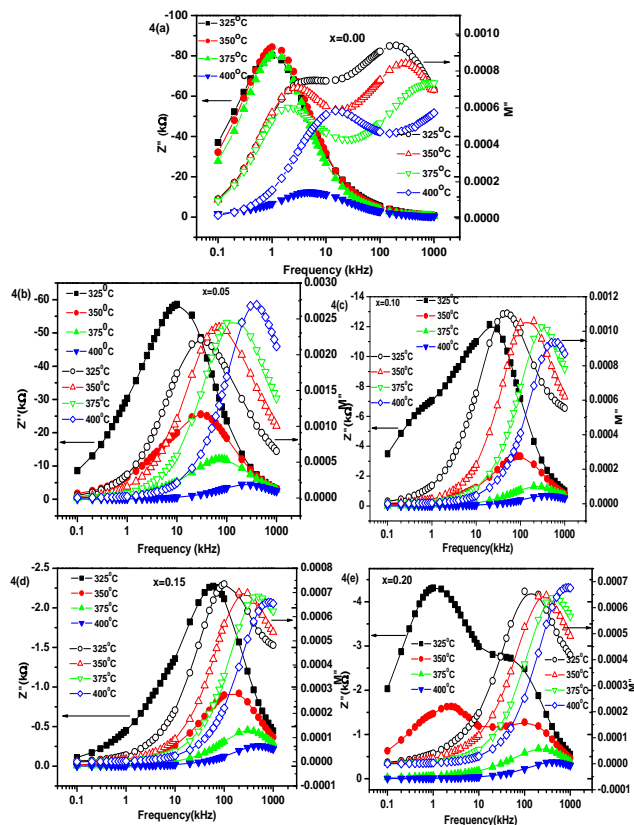
Fig. 4 (a-e). Variation of Z'' and M'' with frequency at different temperature of BiGd$_X$Fe$_{1-X}$O$_3$-PbTiO$_3$ (x=0.00, 0.05, 0.10, 0.15, 0.20).

The value of Z' at each temperature and frequency decreases drastically with increase in Gd concentration up to 0.15. This may be due to the release of space charge at higher frequency side on successive increase of the concentration. The frequency response of M' at different temperature is characterized by very low value of M' in the low frequency region and an increase in the value of M' with the increase in frequency. This may be attributed to the conduction phenomena due to short range mobility of charge carriers.

Fig. 4(**a-e**) shows the variation of Z'' and M'' with frequency at different temperature for all the composites. The magnitude of Z'' increases with increase in frequency and attains a maximum value at a particular frequency and then decreases. The merge of all Z'' curves at higher frequencies indicated the absence of space charge polarization [**35**]. The magnitude of Z'' with a shift in peak towards higher frequency side with rise in temperature confirms the presence of temperature dependent relaxation process in the material. On increasing

the temperature, Z''_{max} and M''_{max} peaks shift towards the higher frequency sides indicate the decrease in relaxation time. Since the peaks of Z''_{max} and M''_{max} do not occur at the same frequency, the relaxation process is mainly due to the short range mobility of charge carriers [**36**]. The maximum relaxation frequency f_{max} corresponding to Z''_{max} helps to evaluate the relaxation time (τ) using a relation $\tau = \dfrac{1}{2\pi f_{max}}$. The variation of τ with inverse of selected temperatures for the concentration x=0.05-0.20 shown in **Fig. 3** [**ESI**]. The nature of the plot appears to follow the Arrhenius relation [**37**] $\tau = \tau_0 \exp(-E_a/K_BT)$, where the symbols have their usual meanings. The values of activation energy calculated from the slope of the curves for the concentration x=0.05-0.20 are shown in **Table 3**. Similarly, the relaxation time has been calculated using the above cited relation from the M''_{max} peak. The variations of relaxation time with inverse of absolute temperature are shown in the **Fig. 3** (**inset**) [**ESI**]. The value of activation energy evaluated (from modulus plot) using the Arrhenius relation mentioned earlier and are given in the **Table 2**.

Table 2. Activation energy (E$_a$ in eV) calculated from impedance, modulus and dc conductivity plots of BG$_x$F$_{1-x}$-PT (x=0.00, 0.05, 0.10, 0.15, 0.20) compounds.

| Sample	E$_a$(Z)	E$_a$(M)	E$_a$(dc)
X=0.00	-----	-----	0.13
X=0.05	1.36	1.22	1.01
X=0.10	1.36	1.02	1.38
X=0.15	0.94	0.99	1.24
X=0.20	1.05	0.99	0.98

The activation energy calculated from modulus and impedance plot are nearly same value. Further, it is observed that the Z''_{max} peak decreases with increase of Gd concentration. This suggests that Gd content in BFO-PT affect the relaxation phenomena in the system. The occurrence of double peaks for concentration x=0.20 shows the grain boundary effect as confirmed from Nyquist plot.

Ac conductivity study

The ac electrical conductivity (σ_{ac}) has been calculated by using an empirical relation $\sigma_{ac}=\omega\varepsilon_r\varepsilon_0\tan\delta$ in order to incorporate the nature of the charge carrier and conduction mechanism in the composite. The notations used in this equation have their usual meaning.

Fig. 5(**a-e**) shows the variation of ac conductivity (σ_{ac}) with frequency of the composites for all the concentration at different temperatures. The conductivity is found to increase with increase in both frequency as well as Gd concentrations. There is an appearance of plateau region in the low frequency side, and hence showing a change in slope at a particular frequency known as hopping frequency. The step like decrease of conductivity on lowering the frequency is observed (at higher temperature) for all concentration. This may be due to the transition from bulk to contact resistance [**38**].
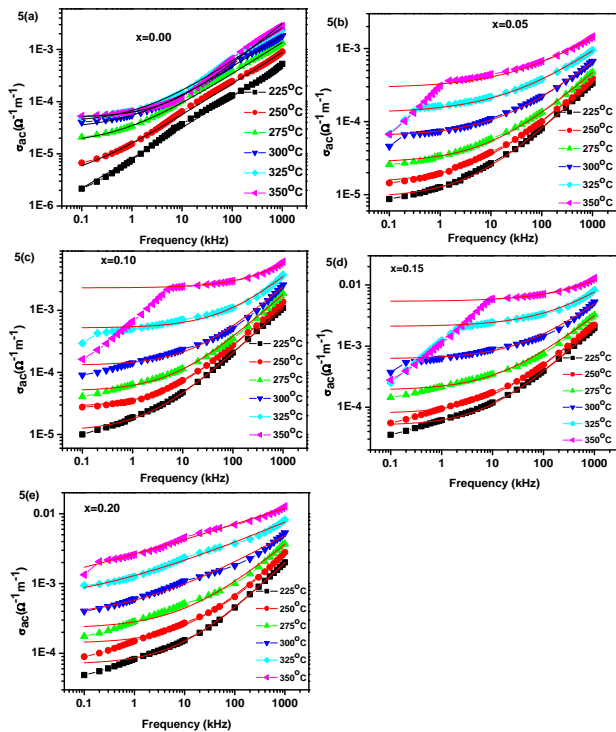
Fig. 5. (a-e). Variation of ac conductivity with frequency of $BiGd_xFe_{1-x}O_3$-$PbTiO_3$ (x=0.00, 0.05, 0.10, 0.15, 0.20) in the temperature range.

This behavior of conductivity spectra follows the universal Jonscher's power law [**39**]: $\sigma(\omega) = \sigma_{dc} + A\omega^n$ where n is the exponent with $0 < n < 1$ and A is the temperature dependent pre-exponential factor defined as $A = \pi N^2 e^2/6k_B T(2\alpha)$ where e=electronic charge, T=temperature, α=polarizability of a pair of sites, N=number of sites per unit volume among which hopping take place. The value of fitted parameters A and n are calculated from the non-linear fit of the Jonscher's power law given in the **Table 2** [**ESI**]. The black solid lines of the fig are the fitted line.

The switch over from σ_0 to σ_{ac} region shows the onset of conductivity relaxation and translation from long range hopping to short range ion motion [**40**]. The value of frequency exponent n were obtained from the Jonscher power law are found to lie between 0.51 to 0.79 for x=0.00-0.15 and 0.23-0.69 for x=0.20 as shown in the **Fig. 4** [**ESI**]. It is observed that the value of n decreases with rise in temperature for all concentration except x=0.00. This behavior of decreasing trend of n with temperature suggests the conduction mechanism in the system and may be due to the correlated hopping of electrons over barrier. Hence, the transport mechanism in BG_xF_{1-x}-PT can be explained by the thermally activated hopping process between two sites separated by an energy barrier. The mechanism for carrier conduction in the sample through the barrier separating the localized sites may be explained by correlated barrier hopping (CBH) model [**41**]. The ac conductivity data have been used to evaluate the density of states at Fermi level $N(E_f)$ using the relation;

$$\sigma_{ac}(\omega) = \frac{\pi}{3} e^2 \omega k_B T \left\{ N(E_f) \right\}^2 \alpha^{-5} \left\{ \ln\left(\frac{f_0}{\omega}\right) \right\}^4$$

where, 'e' is the electronic charge, f_0 is the photon frequency and α is the localized wave function assuming, $f_0 = 10^{13}$ Hz, polarizability $\alpha = 10^{10}$ m^{-1} at various operating frequencies and temperature. **Fig. 6** shows the variation of $N(E_f)$ with frequency at temperatures 350 °C for the samples. It is observed that the values of $N(E_f)$ decreases with increase in the frequency and merge at higher frequency range.
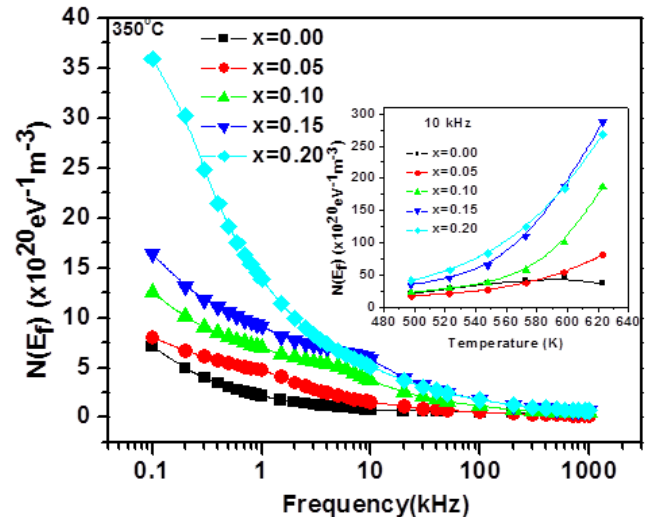
Fig. 6. Variation density of states with frequency as well as temperature (inset) of $BiGd_xFe_{1-x}O_3$-$PbTiO_3$ (x=0.00, 0.05, 0.10, 0.15, 0.20)

Fig. 6 (**inset**) shows the variation of $N(E_f)$ with temperature at frequency 10 kHz for all the samples. It is seen that the $N(E_f)$ increases with the increase in temperature as well as the concentration of Gd. At low frequencies, the electrical conduction in the system is being affected by both frequency as well as temperature, whereas at higher frequencies the charge carriers are localized and being affected by thermal excitations. There is an increase in the density of states with increase in concentration and the reasonably high values of $N(E_f)$ which suggests the hopping between the pairs of sites dominates the mechanism of charge transport in the sample [**42**]. The minimum hopping length, R_{min} was evaluated using the relation $R_{min} = \frac{2e^2}{\pi\varepsilon\varepsilon_0 W_m}$, where $W_m = \frac{6k_B T}{(1-n)}$ is the bonding energy. **Fig. 5** [**ESI**] shows the variation of R_{min} with frequency at temperature 350 °C for all the samples. It is observed that the R_{min} value increases with increase in frequency as well as Gd concentration and having tendency to saturate at high frequency region. A very low value (~10^{-11}m) of R_{min} at low frequency region suggest a lack of restoring force involving the mobility of charge carriers under the action of induced electric field. The R_{min} is increasing sigmoidal nature with increase in frequency and approaching to a constant value, which suggests the conduction phenomena due to short range mobility of charge carrier. **Fig. 5** (**inset**) [**ESI**] shows the variation of R_{min} with temperature at frequency 10 kHz for all the samples. It is observed that R_{min} decreases with increase in temperature.

Dc conductivity

The dc electrical conductivity is evaluated from the impedance data using the relation, $\sigma_{dc} = d/SR_b$ where *d* and *S*

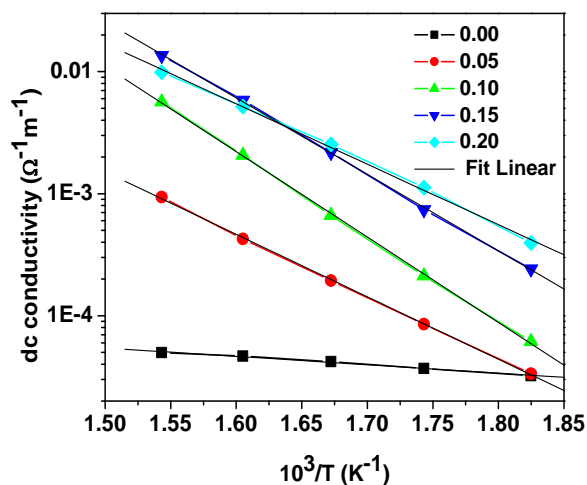are thickness and area of sample respectively, R_b is the bulk resistance.

Fig. 7. Variation of dc conductivity with inverse of temperature of $BiGd_xFe_{1-x}O_3$-$PbTiO_3$ (x=0.00, 0.05, 0.10, 0.15, 0.20)

Fig. 7 shows the variation of dc conductivity with inverse of temperature for all concentration (0.00-0.20). It is found that the dc conductivity increases with rise in temperature for all the samples. The nature of the plot found to obey the Arrhenius relation $\sigma_{dc} = \sigma_0 \exp\left(-E_a/K_BT\right)$.

The value of activation energy calculated from the slope of the plot for all samples given in the **Table 3**.

Conclusion

$0.5BiGd_xFe_{1-x}O_3$-$0.5PbTiO_3$ (x=0.00, 0.05, 0.10, 0.15, 0.20) composites were prepared by a mixed oxide method. X-ray analysis exhibits the tetragonal crystal structure of the composites at room temperature. The c/a ratio decreases from 1.10 to 1.01 with increase in Gd concentration. The values of tolerance factor values of the composite showed the untilted and tilted type perovskite structure. Impedance studies reveal the significant contribution of grain (bulk) and grain boundary effect. The bulk resistance of the material decreases with rise in temperature and exhibits NTCR behavior. The variation of ac and dc conductivity of the material as a function of temperature exhibits Arrhenius type of electrical conductivity. The ac conductivity is found to obey the universal power law and thermally activated conduction process. The activation energy lies in the range 0.13-1.38eV. The correlated barrier hopping (CBH) model has been successfully used to incorporate the electrical conduction mechanism of the sample. The minimum length R_{min} decreases with increase in temperature.

Reference

1. Wang, J.; Neaton, J.B.; Zheng, H.; Nagarajan, V.; Ogale, S.B.; Liu, B.; Viehland, D.; Vaithyanathan, V.; Schlom, D.G.; Waghmare, U.V.; Spaldin, N.A.; Rabe, K.M.; Wuttig, M.; Ramesh, R. *Science,* **2003**, *299*, 1719.
   DOI: 10.1126/science.1080615
2. Hill, N.A.; Filippetti, A.; *J. Magn. Magn Mater.* **2002**, *242*, 976.
   DOI: 10.1016/S0304-8853(01)01078-2
3. Spaldin, N.A.; Friebig, M.; *Science*, **2005**, *309*, 391.
   DOI: 10.1126/science.1113357
4. Smolenskii, G.; Isupov, V.; Agranovskaya, A.; Krainik, N.; *Sov. Phys. Solid State,* **1961**, *2*, 2651.
5. Fischer, P.; Polomskya, M.; Sosnowska, I.; Szymanksi, M.; J. Phys. C. Solid State. **1980**, *13*, 1931.
   DOI: 10.1088/0022-3719/13/10/012
6. Kumar, M. M.; Srinivas, A.; Suryanarayana, S. V.; Bhimasankaram, T.; *Phys. Status Solidi* A, **1998**, *165*, 317.
   DOI:10.1002/(SICI)1521-396X(199801)165:1<317::AID-PSSA317>3.0.CO;2-Y
7. Kanai, T.; Ohkoshi, S.; Nakajima, A.; Watanabe, T.; Hashimoto, K. *Adv. Mater. (Weinheim, Ger.)* **2001**, *7*, 487.
   DOI:10.1002/1521-4095(200104)13:7<487::AID-ADMA487>3.0.CO;2-L
8. Ivanova T. L.; Gagulin, V. V.; *Ferroelectrics,* **2002**, *265*, 241.
   DOI: 10.1080/00150190208260624
9. Mahesh Kumar M.; Srinivas, A.; Suryanarayana, S. V.; *J. Appl. Phys.* **2000**, *87*, 855.
   DOI: 10.1063/1.371953
10. Smith, R.T.; Achenbach, Gary D.; Gerson Robert.; James, W. J. *J.Appl. Phys.* **1968**, *39*, 70.
    DOI: 10.1063/1.1655783
11. Fedulov, S. A. *Dokl. Akad. Nauk SSSR,* **1961**, *139*, 1345.
12. Fedulov, A.; Ladyzhinskii, P. B.; Pyatigorskaya, I. L.; Venevtsev, Y. N.; *Sov. Phys. Solid State,* **1964**, *6*, 375.
13. Sakamoto, W.; Yamazaki, H.; Iwata, A.; Shimura, T.; Yogo, T.; *Jpn. J. Appl. Phys.,* Part 1, **2006**, *45*,7315.
    DOI: 10.1143/JJAP.45.7315
14. Lin, Y.H.; Jiang, Q.; Wang, Y.; Nan, C.W.; Chen L.; Jian Yu: Appl. Phys. Lett. 2007, 90 172507
    DOI: 10.1063/1.4766343
15. Yuan, G.L.; Or, S.W.; Liu J.M.; Liu Z.G. Appl. Phys. Lett. 2006, 89, 052905.
    DOI: 10.1063/1.2266992
16. Emery, S.B.; Cheng, C.J.; Kan, D.; Rueckert, F.J.; Alpay, S.P.; Nagarajan, V.; Takeuchi I.; Wells B.O. *Appl. Phys. Lett.* **2010**, *97*, 152902.
    DOI: 10.1063/1.3481065
17. Kharel, P.; Talebi, S.; Ramachandran, B.; Dixit, A.; Naik, V.M.; Sahana, M.B.; Sudhakar, C.; Naik, R.; Rao M.S.R.; Lawes, G.; *J. Phys. Conds. Matter* **2009**, *21*, 036001.
    DOI: 10.1088/0953-8984/21/3/036001
18. Bing-Cheng, L.; Change-Le, C.; Zhi, X.; Qian, X.; *Phys. Lett. A,* **2010**, *374*, 4265.
    DOI: 10.1016/j.physleta.2010.08.045
19. Zhu, W.M.; Guo, H.Y.; Ye. Z.G. *Phys. Rev. B* **2008**, *78*, 014401.
    DOI: 10.1103/PhysRevB.78.014401
20. Mishra, K.K.; Sarguna, R.M.; Khan S.; Arora, A.K. *AIP Advances.,* **2011**, *1*, 032126.
    DOI:10.1063/1.3624906
21. Burnett, T. L.; Comyn, T.P.; Bell. A.J. *Journal of Crystal Growth*, **2005**, *285*, 156.
    DOI: 10.1016/j.jcrysgro.2005.08.001
22. Heiba, Z.; Okuyucug H.; Hascicek, Y.S. *Journal of Applied Crystallographic,* **2002**, *35*, 577.
    DOI: 10.1107/S0021889802010555
23. Wu. E. *J. Appl. Crystallography,* **1989**, *22,* 506.
    DOI: 10.1107/S0021889889005066

24. Cheng, J.; Shengwen, Y.; Chen, J.; Meng, Z.; Cross, L.E. *Appl. Phys. Lett.,* **2006**, *89*, 122911.
    DOI: 10.1063/1.2353806
25. Patterson A. L. Phy. Rev. **1939**, *56*, 978.
    DOI: 10.1103/PhysRev.56.978
26. Goldschmidt, V. *Naturewissenschaften*, **1926**, *21*, 477
    DOI: 10.1007/bf01507527
27. Fu, W.T.; Visser, D.; Knight, K.S.; IJdo, D.J.W. *J. Solid State Chem.* **2004**, *177*, 1667.
    DOI: 10.1016/j.jssc.2003.12.022
28. Triana, C.A.; Corredor, L.T.; Tellez, D.A. Landınez.; Roa-Rojas, *Materials Research Bulletin,* **2011**, *46*, 2478.
    DOI: 10.1016/j.materresbull.2011.08.024
29. Woodward, David I.; Reaney. Ian M. Acta Crystallogr. **2005**, B*61*, 387.
    DOI: 10.1107/S0108768105015521
30. Reaney, Ian M.; Colla, Enrico L.; Setter, Nava. *Jpn. J. Appl. Phys.* **1994**, *33*, 3984
    DOI: 10.1143/JJAP.33.3984
31. R.D. Shannon, *Acta Cryst*. 1976, *A32*, 751.
    DOI: 10.1107/S0567739476001551
32. MacDonald, J. R. *Impedance Spectroscopy*, *Wiley, New York* **1987**.
    DOI: 10.1002/0471716243
33. Nobre, M.A.L.; Lanfredi, S.; *J.Phys.Chem. Solid,* **2003**, *64*, 2457.
    DOI: 10.1016/j.jpcs.2003.08.007
34. Satpathy, S.K.; Mohanty, N.K.; Behera A.K.; Behera B.; Nayak, P. *Front. Mater. Sci.* **2013**, *7*, 295.
    DOI: 10.1007/s11706-013-0215-7
35. Tilak. B. *American Journal of Materials Science.* **2012**, *2*, 110.
    DOI: 10.5923/j.materials.20120204.03
36. Zhang, S.J.; Alberta, E.F.; Eitel, R.E.; Randall, C.A.; Shrout, T.R. *IEEE Trans. Ultrason. Ferroelectr, Freq. Control,* **2005**, *52*, 2131.
    DOI: 10.1109/TUFFC.2005.1561684
37. Dagdug L.; Garcıa-Colın. L. S.; *J. Phys.: Condens. Matter* **1999**, *11*, 2193.
    DOI: 10.1088/0953-8984/11/10/006
38. Behera, B.; Nayak P. Choudhary, R.N.P, *Cent. Eur. J. Phys*. **2008**, *6*, 289.
    DOI: 10.2478/s11534-008-0030-4
39. Jonscher, A.K. *Nature* **1977**, *267*, 673.
    DOI: 10.1038/267673a0
40. Grigas, J. Microwave dielectric Spectroscopy of ferroelectrics and related materials, *Gordon and Breach Pub. Inc. Amsterdam*, **1996**.
41. Austin, I.G.; Mott N.F. *Adv, Phys*. **1969**, *18*, 41.
    DOI: 10.1080/00018736900101267
42. Bhagat S.; Prasad K. *Phys. Status Solidi A*, **2010**, *207*, 1232.
    DOI: 10.1002/pssa.200925476

Supporting information

**Table 1.** Fitting parameters corresponding to equivalent circuit at 400 ºC of **Fig 3** (a-e).

| Parameters	X=0.00	X=0.05	X=0.10	X=0.15	X=0.20
$R_1(\Omega)$	6.982 x 10^1	2.377 x 10^2	7.685 x 10^1	5.214 x 10^1	6.876 x 10^1
$R_2(\Omega)$	1.334 x 10^3	1.000 x 10^3	1.125 x 10^3	4.504 x 10^2	5.281 x 10^2
$R_3(\Omega)$	3.085 x 10^4	9.403 x 10^3	6.909 x 10^2	7.685 x 10^1	4.544 x 10^2
$R_4(\Omega)$	4.627 x 10^3	1.198 x 10^3	9.803	9.227	2.624 x 10^1
$C_1(F)$	4.126 x 10^{-10}	5.604 x 10^{-11}	2.445 x 10^{-10}	5.522 x 10^{-10}	3.834 x 10^{-10}
$C_2(F)$	3.099 x 10^{-9}	5.593 x 10^{-10}	1.086 x 10^{-12}	3.710 x 10^{-6}	2.602 x 10^{-6}
CPE, Q (S sec$^{0.5}$)	2.296 x 10^{-8}	6.641 x 10^{-8}	6.587 x 10^{-6}	1.155 x 10^{-10}	1.423 x 10^{-6}
Frequency power (n)	6.786 x 10^{-1}	3.729 x 10^{-1}	3.822 x 10^{-1}	4.373 x 10^{-1}	4.933 x 10^{-1}
Warburg,W(S sec$^{0.5}$)	4.017 x 10^{10}	-------------	-------------	-------------	-------------
(χ^2) (Chi squared)	1.339 x 10^{-3}	1.706 x 10^{-5}	5.997 x 10^{-4}	3.089 x 10^{-4}	4.534 x 10^{-4}

**Table 2.** Fitting parameters A and n of the samples obtained from Jonscher's power law at different temperature.

| T(ºC)	x=0.00 A	x=0.00 n	x=0.05 A	x=0.05 n	x=0.10 A	x=0.10 n	x=0.15 A	x=0.15 n	x=0.20 A	x=0.20 n
225	1.26×10^{-7}	0.59	4.51×10^{-8}	0.64	3.89×10^{-8}	0.74	6.58×10^{-8}	0.74	1.35×10^{-7}	0.69
250	2.05×10^{-7}	0.60	7.74×10^{-8}	0.61	5.00×10^{-8}	0.73	1.14×10^{-7}	0.71	2.28×10^{-7}	0.67
275	2.87×10^{-7}	0.61	1.32×10^{-7}	0.58	8.14×10^{-8}	0.72	3.49×10^{-7}	0.65	8.65×10^{-7}	0.59
300	3.37×10^{-7}	0.62	2.07×10^{-7}	0.57	1.10×10^{-7}	0.71	5.46×10^{-7}	0.64	1×10^{-5}	0.41
325	2.98×10^{-7}	0.65	5.74×10^{-7}	0.52	1.84×10^{-7}	0.70	1.31×10^{-6}	0.60	9×10^{-5}	0.31
350	5.53×10^{-8}	0.79	9.13×10^{-7}	0.51	2.29×10^{-7}	0.69	2.11×10^{-6}	0.58	4.2×10^{-4}	0.23
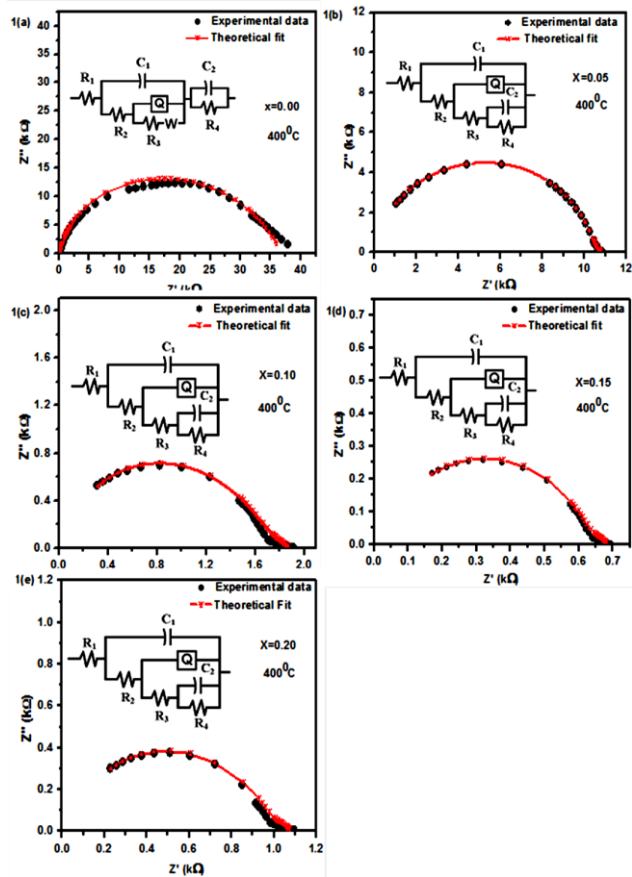
Fig. 1 (a-e). Appropriate equivalent electrical circuit of BiGd$_X$Fe$_{1-X}$O$_3$-PbTiO$_3$ (x=0.00, 0.05, 0.10, 0.15, 0.20) at 400 ºC.
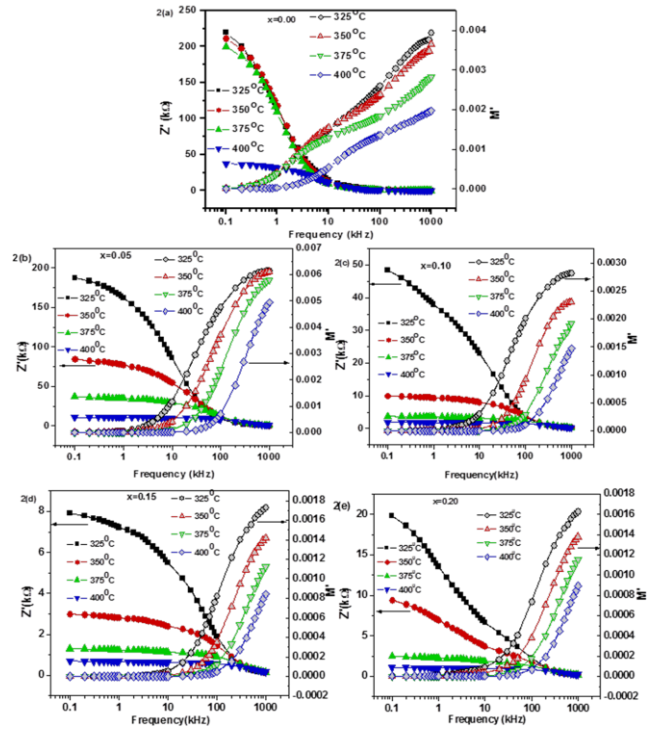
Fig. 2 (a-e) Variation of Z' and M' with frequency at different temperature of BiGd$_X$Fe$_{1-X}$O$_3$-PbTiO$_3$ (x=0.00, 0.05, 0.10, 0.15, 0.20).
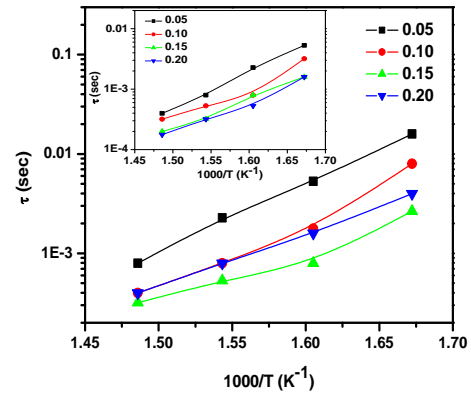
Fig. 3. Variation of relaxation time calculated from impedance plot and from modulus plot (inset) with temperature of BiGd$_X$Fe$_{1-X}$O$_3$-PbTiO$_3$ (x=0.05, 0.10, 0.15, 0.20).
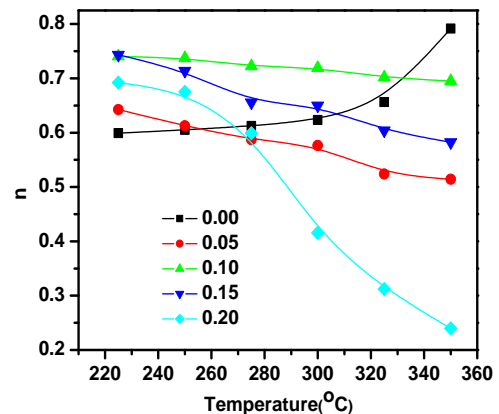
Fig. 4. Variation of n with temperature of BiGd$_X$Fe$_{1-X}$O$_3$-PbTiO$_3$ (x=0.00, 0.05, 0.10, 0.15, 0.20).
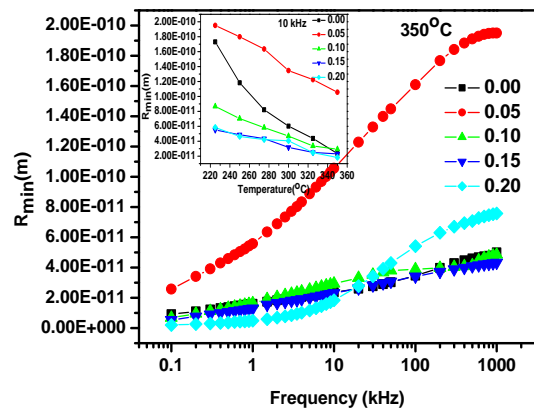
Fig. 5 Variation of hopping length with frequency and temperature (figure inset) of BiGd$_X$Fe$_{1-X}$O$_3$-PbTiO$_3$ (x=0.00, 0.05, 0.10, 0.15, 0.20).